Check for updates

Water Science & Technology

IWA PUBLISHING

© 2021 The Authors

Water Science & Technology Vol 84 No 10-11, 3372 doi: 10.2166/wst.2021.442

Enhanced modelling and experimental validation of ultra-low pressure reverse osmosis membrane system for treatment of synthetic brackish water

Saffa Syamimi Norizam [a], Mohd Azlan Hussain [a,b] and Mohd Usman Mohd Junaidi [a,b,*]

[a] Department of Chemical Engineering, Faculty of Engineering, University Malaya, 50603 Kuala Lumpur, Malaysia
[b] Center for Separation Science and Technology (CSST), Faculty of Engineering, University of Malaya, 50603 Kuala Lumpur, Malaysia
*Corresponding author. E-mail: usmanj@um.edu.my

SSN, 0000-0003-2372-7491; MAH, 0000-0001-8473-1529; MUMJ, 0000-0003-0347-2495

ABSTRACT

Water purification from brackish water sources has been acknowledged as one of the most promising ways to produce drinkable water in water-scarce areas. In this study, an ultra-low pressure reverse osmosis (ULPRO) membrane was numerically and experimentally investigated to produce drinking water by the removal of sodium chloride salt which provides further validation of the model from a practical perspective. An enhanced predictive model based on the Donnan–Steric Pore Model with dielectric exclusion (DSPM-DE) incorporating the osmotic effects was formulated in process simulation. The feed pressure and concentration were optimized as input variables and interaction between them was observed, while salt rejection and water recovery rate were taken as response attributes. The results obtained on the ULPRO membrane showed that the performance depends on the charge, steric, and dielectric effects. Furthermore, the enhanced model was validated with the experimental data attained from a laboratory-scale filtration system with good accuracy in the salt rejection and water recovery results. Comparing the enhanced DSPM-DE with the existing solution diffusion model reveals that the enhanced model predicts the membrane performance better and thereby qualifies itself as a reliable model for desalination of brackish water using ULPRO membrane.

Key words: brackish water, experimental validation, modelling, simulation, ultra-low-pressure membrane

HIGHLIGHTS

- An enhanced DSPM with a dielectric exclusion model for ULPRO membrane is developed.
- Predicted ULPRO membrane performance for low operating pressure of 1 to 4 bar.
- Predicted ULPRO membrane performance for brackish water at salinity up to 2,000 ppm.
- Model validated through experimental data for salt rejection and water recovery with good accuracy.
- Enhanced model predicts salt rejection better than using solution diffusion model.

NOMENCLATURE

A	Active membrane area, m^2
A_k	Mean membrane porosity, %
$C_{i,f}$	Feed ion concentration, mol/m^3
$C_{i,p}$	Permeate ion concentration, mol/m^3
$C_{i,w}$	Membrane wall ion concentration, mol/m^3
c_i	Ion concentration inside the membrane, mol/m^3
$c_{i,0}$	Ion concentration on the feed-membrane surface, mol/m^3
D	Solute diffusivity, m^2/s
D_h	Feed channel hydraulic diameter, m
$D_{i,p}$	Hindered diffusion, m^2/s
$D_{i,\infty}$	Diffusion coefficient of the solute at infinite diffusion, m^2/s
d	Thickness of a layer of oriented water molecules, m
d_e	Diameter of the element, m
e_0	Magnitude of electron charge, C
ε_0	Absolute permittivity of vacuum, F/m

This is an Open Access article distributed under the terms of the Creative Commons Attribution Licence (CC BY 4.0), which permits copying, adaptation and redistribution, provided the original work is properly cited (http://creativecommons.org/licenses/by/4.0/).

Downloaded from http://iwaponline.com/wst/article-pdf/84/10-11/3372/967945/wst084103372.pdf
by guest

ε_f Relative permittivity of solvent in bulk feed
ε_p Relative permittivity of solvent within the pore
ε^* Dielectric constant
F Faraday's constant, C/mol
h_f Feed channel height, m
j_i Ion molar flux, mol/m^2.s
J_w Solvent permeation flux, m^3/m^2.s
k Feed mass transfer coefficient, m/s
k_B Boltzmann constant, 1.38×10^{-23} J/K
$K_{i,c}$ Convection hindrance factor
$K_{i,d}$ Diffusion hindrance factor
$K_{i,\infty}$ Bulk hindrance factor
l Length along the feed channel in the feed flow direction, m
L Membrane length, m
P_f Feed pressure, bar
Q_f Feed flowrate, m^3/h
Q_p Permeate flow rate, m^3/h
R_g Ideal gas constant, J/mol.K
R_i Rejection of ion i, %
Rec Recovery rate, %
r_p Effective pore radius, m
r_i Stokes ion radius, m
T Temperature, K
u Solvent velocity, m/s
v Kinematic viscosity, m^2/s
V_i Partial molar volume of ion i, m^3/mol
x Distance normal to the membrane, m
X_d Effective volumetric membrane charge density, mol/m^3
z_i Charge of individual ion
μ Kinematic viscosity, Pa.s
λ_i Ion radius to membrane pore radius ratio
η Solvent dynamic viscosity within the pore, Pa.s
η_o Solvent dynamic viscosity, Pa.s
ψ Electric potential in the membrane, V
ϕ_i Steric partitioning factor
ϕ_B Born solvation partitioning factor
ΔG_i Gibbs free energy of solvation
$\Delta\Pi$ Osmotic pressure, bar
ΔP Applied pressure drop, bar
Δx Effective membrane layer thickness, m
Sc Schmidt number
Pe_i Peclet number
Re Reynolds number

1. INTRODUCTION

One of the most serious issues impacting individuals around the world is water scarcity, with more than 1.2 billion individuals currently lacking access to clean drinking water (Carolyn *et al.* 2020). Experts predict that by 2030, global water consumption will be 40% higher than its availability (Patrick 2012). Malaysia is not exceptional from this issue, especially in coastal regions and rural areas (Chew *et al.* 2016). In East Malaysia, water stress is much higher compared to West Malaysia, as this area is prone to a long dry season due to monsoonal seasonal changes (Yusof *et al.* 2019). As claimed by the local government, it is a daunting task to provide safe filtered water in the states of the East Malaysia region, as half of its population lives in hilly, rugged and remote rural areas. Under the 12th Malaysia Plan, this state of Sarawak intends to invest RM 18 billion in the next five years to develop more water supply projects (Wong 2020). This shows that the community in Sarawak needs alternative water sources to produce more potable water for the community. The river water in this state of Sarawak may be an ideal place for processing and producing low-cost drinking water using low-pressure membranes as suggested by Manson *et al.* (2018). Approximately 60% of its coastline is covered by mangrove forests (Long 2014) which grow in coastal saline or brackish water. Almost all of the brackish water belongs to channels found in deeper waters that are possibly influenced by the invasion of rivers from Sarawak's mainland rivers such as the Rajang River and Baram River. The heavy tropical area rainfall

Downloaded from http://iwaponline.com/wst/article-pdf/84/10-11/3372/967945/wst084103372.pdf
by guest

is another aspect that could have led to the low salinity of the waters. Therefore, since it is surrounded by vast source of brackish water which has a salinity range from 500 at the estuaries to 30,000 ppm at the nearshore area (Pereira *et al.* 2019), desalting of brackish water is one of the ways to supply communities that have difficulty in accessing freshwater, with potable clean water.

Desalination of brackish water using reverse osmosis (RO) has been one of the ultimate effective methods for addressing water scarcity (Pan *et al.* 2020). Unfortunately, this technology is costly, less acceptable, and unaffordable for many countries (Kausley *et al.* 2018). It is an extensive energy process as the range for desalination of brackish water using the RO process is from 17 to 27 bar (Kondili 2012) which is considerably high and thus can result in high capital costs, as well as a high level of labor competence to manage such a huge infrastructure (Shenvi *et al.* 2015). Due to these drawbacks, developing countries such as Malaysia cannot afford to apply this technology and the development of such water treatment facilities may be hindered. This process can be improved further with the development of membranes that are more energy efficient and easier to operate compared to current technologies (Ozaki *et al.* 2000).

The energy extensive and cost-prohibitive nature of RO membranes as pressure-driven systems has led to the advent of the ultra-low pressure reverse osmosis (ULPRO) membrane, which offers a viable alternative as it is able to remove certain solutes from water as effectively as the RO, while using far less operating pressure (less than 5 bar) (Ozaki 2004; Xu *et al.* 2008). The ULPRO membrane has been classified under the category of nanofiltration (NF) due to its porous characteristic (Ozaki 2004). However, it is upgraded over other commercial low-pressure NF membranes in solute dismissal and flux advancement (Prayoga *et al.* 2021). The ULPRO membrane produces twice the flux of the existing composite RO membrane at a lower working pressure, while maintaining a high removal degree of salt and organic compounds (Ozaki *et al.* 2000; Prayoga *et al.* 2021). It is developed as an energy-saving membrane (Gerard *et al.* 1998) with selectivity properties of fractionating low-molecular-weight ions of different values and high water permeability (Hilal *et al.* 2004). In addition, the ULPRO membrane is also capable of removing both anionic and cationic pollutants together with organic compounds of molecular weight cut-off (MCWO) 200–400 Da (Nguyen *et al.* 2013; Imbrogno & Schäfer 2019; Hafiz *et al.* 2021). Subsequently, ULPRO is a good alternative for treating and processing brackish water for a variety of industrial applications including drinking water production (Van der Bruggen & Vandecasteele 2003).

The capability to estimate the efficiency of ULPRO membrane rejection is essential in process design and operation. Both structural and functional criteria such as the effective pore radius, the active layer thickness to membrane porosity ratio, the permeability of the membrane towards certain salts, and the electrical properties, in particular membrane charge density, are often used to describe NF membranes (Micari *et al.* 2020). In this study, an NF-based model, specifically Donnan–Steric Pore Model with dielectric exclusion (DSPM-DE) is employed as the basis to formulate the ULPRO system model. One of the limitations of the previous research using this DSPM-DE model was that the rejections of ions were predicted on a specified flux without accounting for the osmotic effects for high salt concentration solution (Mohammad *et al.* 2007). Since brackish water and the ULPRO membrane system is used in this study, the osmotic effect induced by salt concentrations at the membrane wall is expected to influence the flux inside the membrane system, considering that the ULPRO membrane has a smaller pore radius compared to other low-pressure NF membranes. As the membrane pore size is relatively smaller, the osmotic pressure difference will affect the flux inside the membrane. Since NF membrane usually rejects most of the divalent ions (70–90%) while monovalent ions such as sodium ion, Na^+ and chloride ion, Cl^- are only rejected to a certain percentage (30–80%) (Van der Bruggen *et al.* 2004; Mukherjee 2014), these monovalent ions may influence the observed rejections and thus affect the overall osmotic pressure in the ULPRO membrane. This shows that comprehensive modelling and simulation studies that are validated experimentally are essential to understand the transport mechanism of solute inside the ULPRO membrane. Such analysis would provide a deeper understanding of the influence of the membrane properties and feed condition on the membrane system performance (Chew *et al.* 2016).

Therefore, the primary goal of the contribution in this work is to develop an experimentally validated enhanced DSPM-DE model for the ULPRO membrane system by considering the osmotic effects to simulate the process to further improve its predictive performance outcome, which will aid to further understanding to users in the mechanism of the ULPRO process. From the enhanced formulated model, the effect of applied pressure and salinity are examined for its salt rejection and water recovery performances and validated with data obtained from actual laboratory experiments. Comparison with the existing solution diffusion model to show the superiority of the enhanced model has also been carried out.

Downloaded from http://iwaponline.com/wst/article-pdf/84/10-11/3372/967945/wst084103372.pdf
by guest

2. ENHANCED MODEL OF ULPRO MEMBRANE SYSTEM

In this work, the enhanced DPSM-DE model formulated is an improved model to the original DSPM which accounts for Donnan, dielectric, and steric exclusion effects by solving the Extended Nernst–Planck (ENP) equation for each solute species inside the membrane system using the boundary conditions at the membrane wall (Roy & Sharqawy 2015). This DSPM-DE model is found to be particularly effective in predicting the rejection ion Ca^{2+} and Mg^{2+} according to Bowen & Welfoot (2002b). Researchers who have recently developed a model for the NF system have also employed this DSPM-DE model which showed great reliability in predicting the membrane performance (Agboola *et al.* 2015; Roy & Sharqawy 2015). For most NF systems, this dielectric exclusion mechanism dominates other mechanisms used to describe the dielectric exclusion, which involves image charges that build at the bulk solution–membrane interface (Bowen & Mohammad 1998; Bowen & Welfoot 2002a). The schematic diagram of the coordinate system employed is shown in Figure S.1 in the supplementary materials. In this work, sodium chloride (NaCl) salt is used to represent the salinity since dissolved ions in brackish water are comprised mainly of Na^+ and Cl^- ions (Gray *et al.* 2011).

The assumptions below were applied for the development of the model equations (Bowen & Yousef 2003; Agboola *et al.* 2015):

- The solution is assumed to behave ideally.
- The solute is assumed to be spherical in shape.
- The transport mechanism inside the pore is governed by diffusion, electromigration, and convection.
- The 'restricted' transport is defined by incorporating the hindrance factors for diffusion and for convection.
- The flow inside the pore is considered to be laminar and Hagen–Poiseuille model is applied to determine the velocity of the solvent.
- Operating pressure affects the chemical potential of the solute.
- Solvent inside the pores is composed of a layer of oriented water particles.
- Variation of dielectric constant and viscosity of solvent in the pore is factored into equations.
- The membrane's surface concentration polarization is neglected.
- Concentration does not influence the diffusion coefficient and partial molar volume inside the pore.
- The pore interface separation is caused by steric, Donnan effect, and dielectric exclusion.
- The electroviscous term for the ion's velocity within the solvent is neglected.
- Axial variation of the concentration and potential gradient is applied, while radial variation is neglected.

Based on those assumptions, the main modelling equations are formulated which consists of Equation (1) to (29) can be referred to Table S.1 in the supplementary materials. The ENP in Equation (1) describes the molar flux of ion i involving the three main mechanisms of ion transport: diffusion (owing to the concentration gradient), electromigration (owing to the electric potential gradient), and convective forces (owing to the pressure gradient) correspondingly. The hindered diffusivity coefficient of ion, $D_{i,p}$ in Equation (1) is the diffusivity of salt inside the pore and is obtained through Equation (2). The diffusion coefficient of NaCl at infinite diffusion, $D_{i,\infty}$ is 16.1 m^2/s (Imbrogno & Schäfer 2019) which is obtained from the Wilke–Chang equation (Fei & Bart 2001). The hindered nature of ion transportation in the NF membrane due to extremely small pore size (Anderson & Quinn 1974; Davidson & Deen 1988) is represented as diffusion hindrance factor, $K_{i,d}$ and convection hindrance factor, $K_{i,c}$ in Equations (3) and (4). The diffusion and convection hindrance factors are controlled by the coefficient of steric partitioning, ϕ_i which is the relation between the boundary conditions for concentration in the feed-membrane interface. $K_{i,d}$ and $K_{i,c}$ are determined by calculating the ion-to-pore radii ratio as shown in Equation (5). The ionic radii, r_i is obtained from Stokes' radius from the Stokes–Einstein equation in Equation (6) (Deen 1987) which is 0.13 nm for NaCl (Imbrogno & Schäfer 2019).

Moreover, since the solute is considered to be spherical in shape, Stokes' radius is predominantly viewed as the best parameter to represent the solute size (Davidson & Deen 1988). Born solvation energy, ϕ_B which is also contributing to the partitioning as shown in Equation (7) is calculated using Gibbs' free energy of solvation, ΔG_i in Equation (8) that was derived from the Born model (Hussain *et al.* 2006). The change of viscosity inside the pore that is required to determine the pore diffusion coefficient, $D_{i,p}$ is obtained through Equation (8). The average pore dielectric, ε_p is calculated as described in Equation (10) by guessing that oriented water particles layer with the thickness, d and dielectric constant ε^* is coating the pore wall and the interior section of the pore has the relative permittivity of solvent in bulk feed, ε_f taken as 78.4, which is the value of pure water dielectric constant at room temperature (Ellison 2007).

Downloaded from http://iwaponline.com/wst/article-pdf/84/10-11/3372/967945/wst084103372.pdf
by guest

The mass transfer coefficient, k_i for spiral wound membrane as shown in Equation (11) is determined once the dimensionless Schmidt number (Equation 12) and the Peclet number (Equation 13) are calculated. Moreover, the pressure drop of the membrane system is obtained through Equation (14) by first determining the friction factor and the Reynolds number as shown in Equation (15). Since the ion concentrations are restricted by the electroneutrality condition in Equations (16) to (18), it can be written as the concentration gradient of individual ions, c_i by Equation (19) while the electric potential gradient is presented by Equation (20). The partitioning of ions at the membrane interface which is caused by the steric effect (ϕ_i), Donnan exclusion effect ($\Delta\psi_{D,0}$), and the dielectric exclusion effect ($\Delta W_{i,0}$) is described by Equation (21). The Hagen–Poiseuille equation is used to compute the transmembrane solvent flow in Equation (22) and determine the relationship between applied pressure and permeate flux.

Since the osmotic effect is considered in this work, the Van 't Hoff equation is incorporated into the DSPM-DE model to calculate the osmotic pressure and the permeate flux due to its simplicity, as shown in Equation (23). The salt rejection and the ion recovery rate for species *i* are given by Equations (24) and (25). To solve the model equations, boundary conditions for each ion concentration in the feed and permeate sides are defined as Equations (26) and (27). Lastly, the feed and permeate Donnan potential can be denoted by using Equations (28) and (29) respectively.

3. METHODOLOGY

The procedures in this analysis are divided into two sections: (1) modelling and simulation steps, and (2) experimental steps. The main equations used in the enhanced model are summarized in Table S.1 in supplementary materials and the modelling and simulation details are given in Section 3.1. Next, the experiments are carried out by using the Vontron ULPRO membrane (ULP32-8040) and the steps in performing the experiments are discussed in detail in Section 3.2.

3.1. Modelling and simulation

In this study, the ULPRO membrane (ULP32-8040) manufactured by Vontron Technology Ltd was utilized. Since this Vontron ULP32-8040 membrane is only applicable for salt concentration up to 2,000 ppm (Vontron 2016), the salinity of the brackish water is simulated from 500 ppm to 2,000 ppm only. The ULPRO membrane module is made of synthetic aromatic polyamide in the spiral wound configuration with a stable rejection rate at 95%, average permeate flow at 39.7 m^3/day, effective membrane area of 37 m^2, and operating pressure up to 41.4 bar (Vontron 2016). The general parameters such as active membrane area and the operating conditions are listed in Table 1. The model equations in Table S.1 were simultaneously solved to predict the salt rejection and the water recovery rate.

A programming and numeric computing platform called MATLAB 7.7 (R2011b) was utilized to solve the model equations. A flow chart of the enhanced model integration, which describes the structure and steps to integrate, calculate and solve the model equations, is shown in Figure S.2 in the supplementary materials. The component fluxes and concentration profiles inside the membrane could not be solved independently in these models. As a result, the problem-solving process has to be iterative.

First, the model equations for the feed-membrane interface, the membrane active layer and the membrane-permeate interface were linearized. Based on the linearized equations, a degree-of-freedom analysis was carried out to ensure that the simulation problem is well posed (Geraldes & Alves 2008). The required operating conditions were set and the necessary parameters such as hindrance factors, pore diffusion coefficient and mass transfer coefficient were calculated first before solving the non-linear ordinary differential equations (ODE). The solution of the model starts with an initial guess for $C_{i,p}$ values of each solute. In this way, the ODEs as shown in Equations (13) and (14) in Table S.1 formed by the concentration gradient can be integrated over the boundary layer and membrane thickness to get the new $C_{i,p}$ values,. In addition, since J_w are dependent on $C_{i,w}$ due to the osmotic pressure difference, an internal loop was needed to solve the equations. This value must be recalculated at each iteration step. In order to solve the fourth-order non-linear ODEs, the implicit Runge–Kutta algorithm using the Newton–Raphson method was applied (Xie 2011) to solve the relationship of the membrane-permeate concentration. The simulation ended when the concentrations of membrane wall and the permeate converged and the required TDS level for drinking water which is 300 ppm according to WHO Guidelines for Drinking-water Quality was achieved (WHO 2011).

3.2. Experiment

Experiments were conducted in a single pass open circuit as shown in Figure 1 with the cross-flow mode of operation using Vontron's ULP32-8,040 membrane module. The primary components in the production of drinkable water in this analysis are

Downloaded from http://iwaponline.com/wst/article-pdf/84/10-11/3372/967945/wst084103372.pdf
by guest

Table 1 | Modelling parameter and the operating conditions

Parameter	Value
Feed condition	
Feed temperature, T_f (°C)	26
Feed pressure, P_f (bar)	1, 2, 3 & 4
Feed flowrate, Q_f (m^3/h)	0.04
Feed concentration, C_f (ppm)	500, 1,000, 1,500 and 2,000
Feed pH	6
Solvent velocity, u_w (m/s)	0.5
Water properties	
Density of water, ρ_w (kg/m^3)	998
Dynamic viscosity of water, η_w (N.s/m^2)	0.89×10^3
Kinematic viscosity of water, v_w (m^2/s)	0.91×10^3
Diffusivity of water, D_w (m^2/s)	1.2×10^{-9}
Sodium Chloride (NaCl) properties	
Osmotic coefficient of NaCl	0.93
Molecular weight of NaCl, MW (g/mol)	58.4
Diffusivity of NaCl, D (m^2/s)	1.34×10^{-9}
Average density of NaCl, ρ (kg/m^3)	1,010 at 26 °C
Dynamic viscosity of NaCl, η (N.s/m^2)	0.0007
Kinematic viscosity of NaCl, v (m^2/s)	9.2×10^{-7}
Membrane characteristics	
Membrane type	ULP32-8040
Length, L (m)	1[a]
Active membrane area, A (m^2)	37[a]
Diameter of element, d_e (m)	0.2[a]
Length along the feed channel in the feed flow direction, l (m)	1.016
Hydraulic diameter of the feed channel, D_h (m)	0.2019
Feed channel height, h_f (m)	0.5
Mixing length of the spacer, L_{mix} (m)	1

[a]Reference: Vontron (2016).

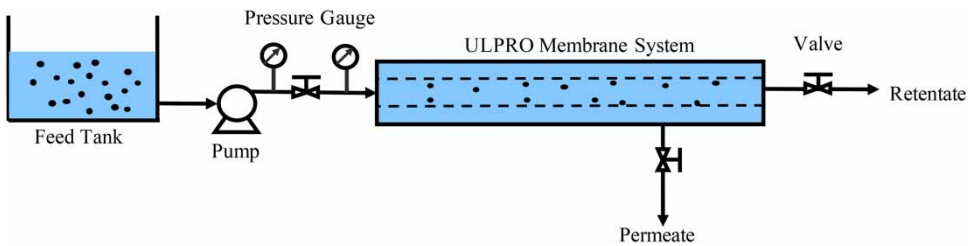

Figure 1 | Schematic diagram of brackish water treatment system in a cross-flow configuration.

a feed tank, a pump unit, and the ULPRO membrane system. Different pieces of piping, a flow meter, valves, and connectors complete the setup. A permeability test was first performed to measure the pure water permeability (PWP) by assuming the osmotic pressure difference to be zero. Pure water flux was determined by using the transmembrane solvent flux as described

Downloaded from http://iwaponline.com/wst/article-pdf/84/10-11/3372/967945/wst084103372.pdf
by guest

in Equation (16) in Table S.1. Experiments with pure water were carried out with varied transmembrane pressures (TMP) to determine the pore size for the membrane's active surface by evaluating the flux inside the membrane system.

By changing the applied feed pressure from 1 bar to 4 bar, the permeate and the retentate flow were calculated at different feed concentrations (500 to 2,000 ppm). The salt rejection and the water recovery rate of the membrane were computed by using Equations (18) and (19) in Table S.1.

The conductivity of the feed and permeate solutions were measured at room temperature using a conductivity meter to obtain the salt concentration. The permeate flow rate was measured with a measuring cylinder, a high-accuracy balance and a stopwatch. After every run, the system was thoroughly backwashed with clean water for several minutes and completely drained afterward. Every experiment of filtration was repeated at least twice to achieve acceptable reproducibility.

4. RESULTS AND DISCUSSION

4.1. Simulation results

In the simulation study, the effect of the performance of the membrane system based on salt rejection and water recovery rate has been carried out. The rejection performance of the ULPRO membrane was analyzed as a function of its structural and electrical characteristics, which is beneficial to both theoretical and membrane characterization studies.

4.1.1. Effect of applied pressure on salt rejection

Based on the computational model, the relationship of applied pressure with the salt rejection is displayed in Figure 2. The permeate salt concentration decreased with increasing applied pressure due to the rise of the preferential sorption of the membrane surface for pure water at higher operating pressure. According to Abidi *et al.* (2016), Na^+ ions are able to partially get caught and trapped inside the membrane pores with a diameter of around 1 nm by the surface forces of the membrane which include friction forces and electrostatic forces. This showed that the diffusive solvent transport via membrane in this study is lower than convective transport at high operating pressure. The convective transport becomes the governing mechanism that allows the permeate salt concentration to decrease as the applied pressure goes up (Chai *et al.* 1997). Moreover, the membrane is considered as a negatively charged membrane at operating pH range of 3 to 10 during continuous

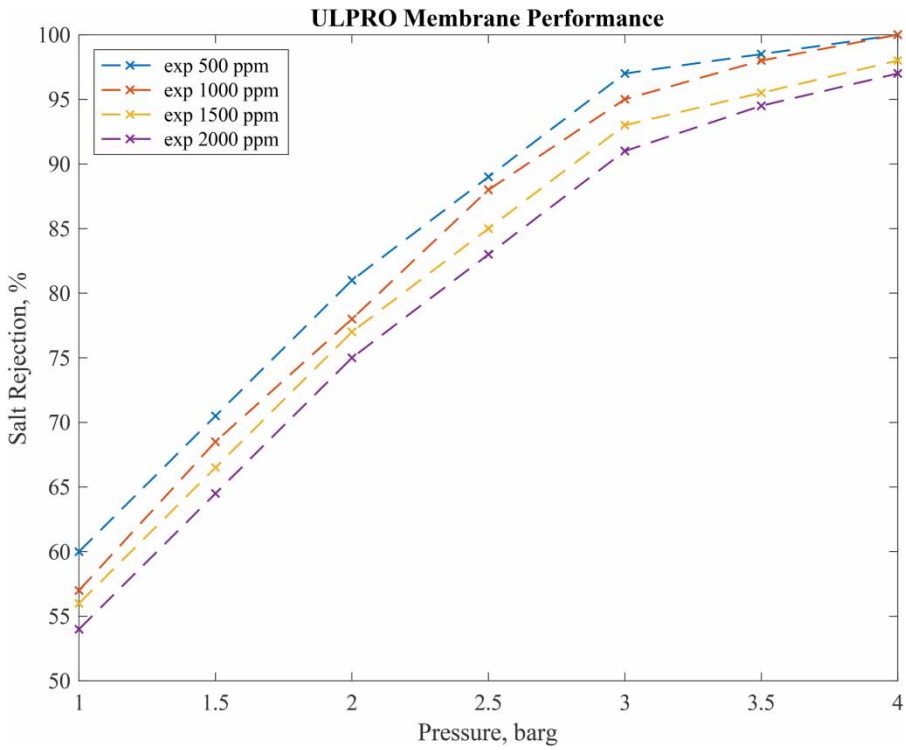

Figure 2 | Effect of applied pressure on the simulation salt rejection of the ULPRO membrane.

Downloaded from http://iwaponline.com/wst/article-pdf/84/10-11/3372/967945/wst084103372.pdf
by guest

operation (Abidi *et al.* 2016; Vontron 2016). The surface forces remain constant while the water flux continues to increase with the feed pressure and thus causing the permeate concentration to decrease and the salt rejection to increase (Abidi *et al.* 2016).

When Born's effective radius was implemented, the degree of rejection for positive charge ion showed a slight increase compared with the negative ion, as the sodium ion size is smaller than the chloride ion (Hussain *et al.* 2006). Moreover, it was observable that the Donnan distribution is predominant compared to the steric effects when using Born's effective radii. In addition, the Donnan factor, which is contributed by effective membrane charge density played a significant role in the membrane transport mechanism and thus described this ULPRO membrane as having a tight membrane structure (Ali *et al.* 2014). From these observations, the desired membrane separation performance is more favorable for membranes with high Donnan factors with smaller membrane pore sizes (Sidek *et al.* 2014).

4.1.2. Effect of applied pressure on water recovery rate

Based on the model that has been solved using MATLAB, the relationship of applied pressure with the water recovery is displayed in Figure 3. The graph shows a linear relationship between the applied pressure and the recovery rate. The recovery percentage is inversely proportional to permeate flow rate and rejection percentage given other parameters such as TDS feed water, operating pressure, and temperature of the feed water remains the same.

4.2 Experimental results

4.2.1. ULPRO membrane characteristics

Based on the experiments, PWP was obtained as the slope of the linear relationship between applied pressure and the pure water permeate flux (Baker 2012) and determined to be 6.47 ± 1.5 L/m^2.h.bar. By comparing the water permeability flux of this ULPRO membrane with other commercialized membranes as shown in Table 2, it can be seen that this ULPRO Vontron ULP32-8040 membrane used in this has a lower permeability value than the NF-90 and the NF-270. This value describes the characteristic of the membrane as having a small pore size and low porosity.

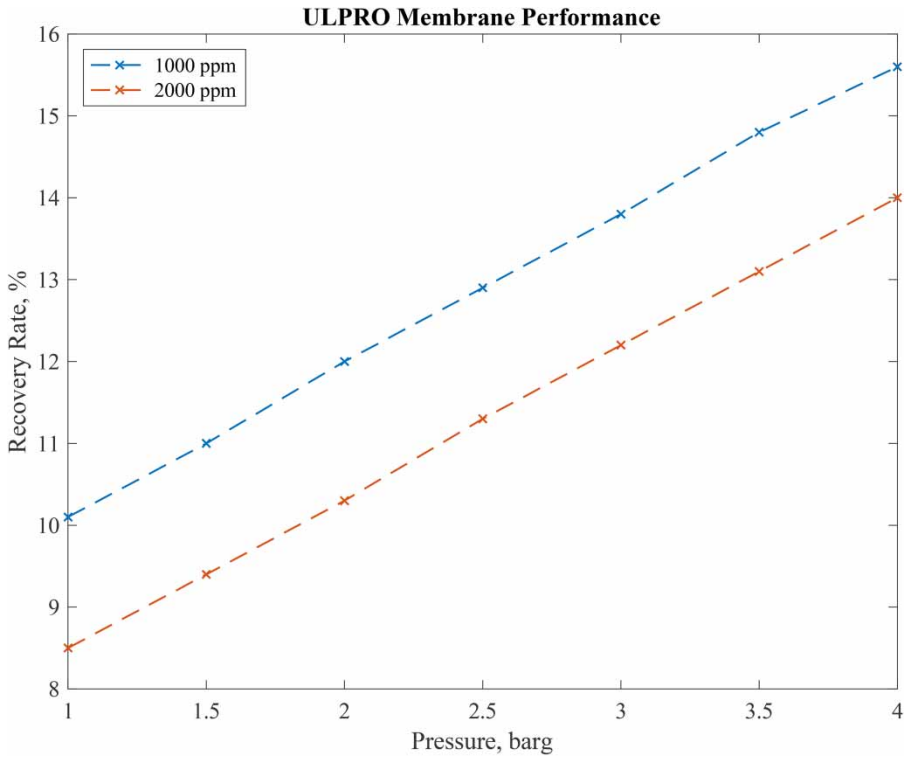

Figure 3 | Effect of applied pressure on the simulation water recovery rate of the ULPRO membrane at NaCl concentrations of 1,000 ppm and 2,000 ppm.

Downloaded from http://iwaponline.com/wst/article-pdf/84/10-11/3372/967945/wst084103372.pdf
by guest

Table 2 | Pore size of the various membrane and its percentage difference with Vontron ULP32-8040 membrane

ULPRO membrane	PWP (L/m².h.bar)	Mean pore radius (nm)	Pore size difference (%)
ULP32-8040 (Vontron)	6.47 ± 1.5	0.33	n.a.
NF-90 (tight) (Dow/Filmtec)	8 ± 2[a]	0.35[a]	+ 6
NF-270 (loose) (Dow/Filmtec)	14 ± 2[a]	0.40[a]	+ 21

n.a. Not applicable.
[a]Reference: Imbrogno & Schäfer (2019).

The membrane-specific parameters such as the membrane effective pore radius, the pore dielectric constant, the membrane volumetric charge density, and the ratio of the membrane active layer thickness to porosity were determined by comparing model calculations with existing ULPRO data. The average pore radius of the membrane, r_p is determined to be 0.33 nm by fitting the experimental data to the results of the enhanced DSPM-DE model. It can be seen from data in Table 2 that this Vontron ULPRO membrane is a tight NF membrane as its mean pore radius is less than NF-90. Subsequently, the active membrane thickness, Δx can be simply calculated by determining the slope in Equation (22) in Table S.1 as a function of the measured effective pore radius, i.e. $\frac{\Delta x}{A_k} = \frac{r_p^2}{slope}$ (Dalwani *et al.* 2011; Baker 2012). The calculated active layer thickness to porosity ratio, $\Delta x/A_k$ was about 1 μm. Next, the ratio of ion radius to membrane pore radius, λ_i was calculated and found to be 1.84 and 1.21 for Na^+ and Cl^-ions, respectively. In addition, by fitting with experiments with NaCl rejection data (Oatley *et al.* 2012; Roy & Sharqawy 2015), the ULP32-8040 membrane has a pore dielectric constant, ε_p of 38. The membrane volumetric charge density, X_d was determined to be 34 mol/m^3 by fitting to the concentration of solute, the pH of the solution and the nature of solute and solvent explicitly. Therefore, this ULPRO membrane can be considered as having high λ_i and low X_d, and is classified under the NF membrane system that has a high membrane structure with low membrane charge density.

Indeed, it can be seen that the value of the parameters shown in Table 3 which are used in characterizing a membrane can be considered to be unique for the ULPRO membrane. The first three parameters are unaffected by the amount of salt in the feed, the pH of the solution, or the type of the solute (Bowen & Mohammad 1998). However, if any of these parameters are fitted to data for other solutes, these values may change slightly (Bowen & Mohammad 1998; Bowen & Welfoot 2002a; Oatley *et al.* 2012).

4.2.2. Effect of applied pressure on salt rejection

The performance of the ULPRO membrane is evaluated under different operating pressures. The easiest technique to measure the salinity is by measuring the conductivity of the feed and the permeate. The experiment data collected were converted from conductivity to concentration through the relationship of 1 μS/cm equivalent to 0.64 ppm.

Based on the experiments, the effect of operating pressure on the salt rejection rate with its standard deviation at room temperature (26 °C) is shown in Figure 4. It was discovered that, as the feed pressure increased, the salt rejection and the permeation flux increased. At the feed pressure of 4 bar, the membrane rejected more salt that flowed through the brine stream, while less salt passed through the membrane to the permeate stream with a rejection rate of 99 ± 1% for 500 and 1,000 ppm salt concentration, 98% ± 1 for 1,500 ppm and 97% ± 1 for 2,000 ppm. These promising values for water treatment application could be described by the steric hindrance mechanism and the effect of the Donnan factor due to the fact that this ULPRO has a relatively small pore size. These two effects which play a significant role in tight membrane structure and for membrane of having strong ion repulsion by the membrane charge density, causes the salt rejection performance to

Table 3 | Membrane characterization parameters

Parameter	Value
r_p	0.33 nm
$\frac{\Delta x}{A_k}$	1 μm
ε_p	38
X_d	34 mol/m^3

Downloaded from http://iwaponline.com/wst/article-pdf/84/10-11/3372/967945/wst084103372.pdf
by guest

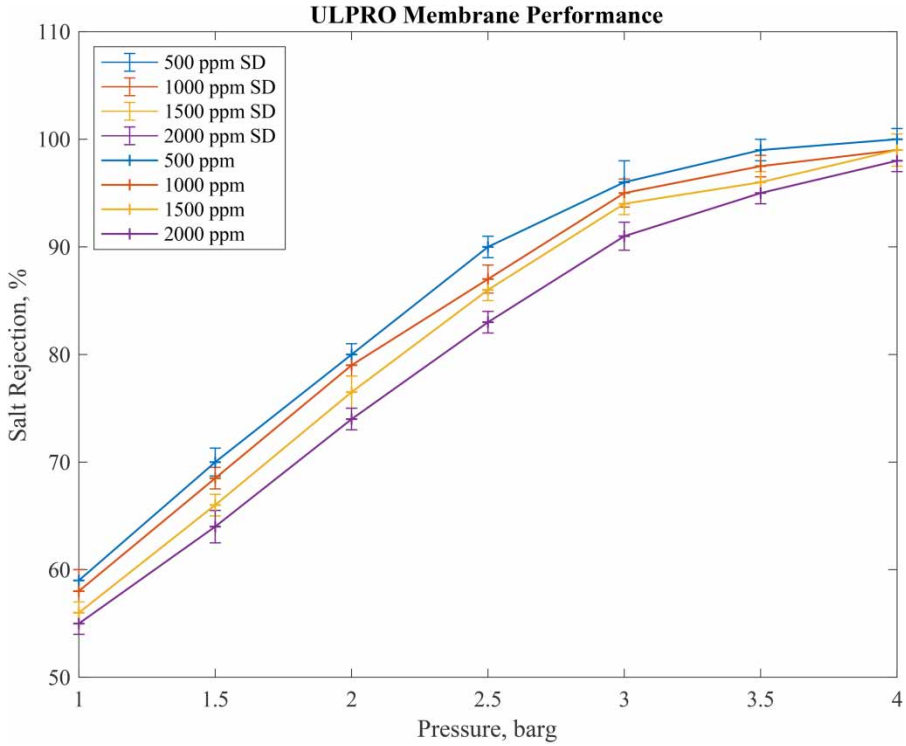

Figure 4 | Effect of applied pressure on the experimental salt rejection of the ULPRO membrane.

increase as shown by Ali *et al.* (2014) and Bowen & Mohammad (1998) under a hindrance factor mechanism. Likewise, the salt diffusive transport across the membrane is greater than that of convective transport at low feed pressure. Convective transport becomes increasingly significant as the applied pressure increases, allowing the ion concentration in the permeate to drop (Chai *et al.* 1997).

4.2.3. Effect of applied pressure on water recovery rate

Based on the experiments done in this study, the relationship of applied pressure with the water recovery is showed in Figure 5 for the concentration of 1,000 and 2,000 ppm. With the increase of feed concentration, the permeate flow and recovery rate have shown a reduced pattern. A factor that contributes to this outcome is that as the salt concentration in the feed water increases, the osmotic pressure becomes increased too and thus causing the effective pore radius of the membrane to become decreased due to the solute adsorption on the membrane surface, and the influence of concentration polarization. This result is in agreement with findings obtained by Ahn *et al.* (1999). The change in water recovery rate for this membrane is not very significant as the feed pressure increases and it is relatively low compared to other brackish water desalination membranes, which commonly achieve a 50% to 75% recovery rate. The low value of the water recovery rate can be due to having no recycling of the retentate back into the system. It is believed that the recycling system can help to produce more permeate flow and thus results in a high water recovery rate compared with the normal rate of 50% to 75%.

Figure 5 shows that the water recovery rate increases linearly from 1 bar to 3 bar and starts to show slow increment starting at 3.5 bar to 4 bar. The graph is compatible with the theory that as the feed pressure increases, more permeate water is produced and thus gives a higher water recovery rate. However, the slow increment at 3.5 bar to 4 bar is likely to have been caused by the internal concentration polarization (Obotey Ezugbe & Rathilal 2020) which describes the accumulation of ions in the boundary layer. It elevates the osmotic pressure at the top of the membrane, causing a reduction in the solvent permeation flux, J_w (Koseoglu *et al.* 2018), and thus resulting in the permeate flow to decrease as well. However, the higher applied pressure moderately overcomes this phenomenon which causes the recovery rate to increase slowly.

Fundamentally, the maximum water recovery of the ULPRO membrane is determined by the concentration of salt in the feedwater and the potential of salts to precipitate on the membrane surface rather than by the osmotic pressure. From Figure 5, the recovery rate for feedwater with lower salt concentration is higher than feedwater with higher salt content;

Downloaded from http://iwaponline.com/wst/article-pdf/84/10-11/3372/967945/wst084103372.pdf
by guest

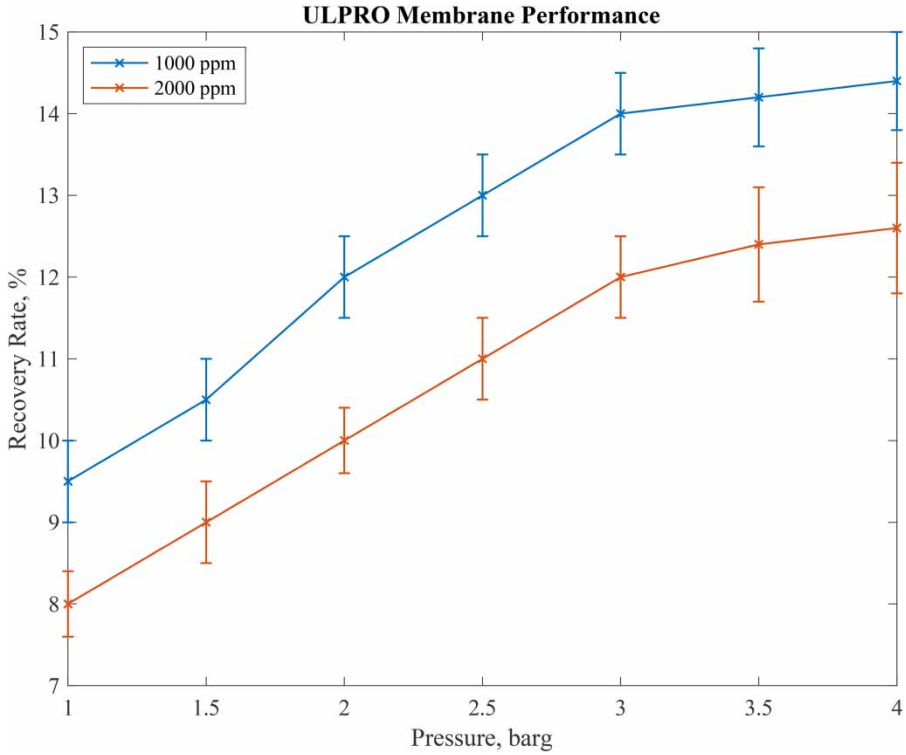

Figure 5 | Effect of applied pressure on the experimental water recovery of the ULPRO membrane at NaCl concentrations of 1,000 ppm and 2,000 ppm.

for example, at 4 bar, the recovery rate for 1,000 ppm and 2,000 ppm salinity is 14.4% and 12.4%, respectively. Based on the manual provided by Vontron (Vontron 2016), this membrane normally achieved a 15% recovery rate during the test with 2,000 ppm of salt concentration at 10 bar. Therefore, these values of the water recovery rate at different feed pressure obtained in this experiment can be considered to be acceptable at different pressures..

4.3. Comparison between simulation and experimental result

The simulation results of the enhanced model were validated and compared with the experimental data for various concentrations of NaCl at different feed pressure, as shown in Figure 6. The mean squared error for salt rejection between these two results was calculated and found to be 0.6. The model prediction was demonstrated to be in good agreement with the experiment results.

Comparison between simulation and experimental results for water recovery rate has also been made. In Figure 7, the impact of feed pressure on recovery rate is shown for 1,000 ppm and 2,000 ppm salt concentrations. The simulation and the experimental results show a similar pattern at 1 bar to 3 bars. However, the experimental data starting from 3.5 bar show a slow increment in the recovery rate. This is due to the internal concentration polarization (Obotey Ezugbe & Rathilal 2020) that causes the flux to reduce but the high applied pressure somewhat overcomes it, as mentioned earlier. The mean squared error for recovery rate between these two results was calculated and found to be 0.5. Although the recovery rate from experimental results starts to increased slowly starting at 3.5 bar, the mean squared error is still considered to be small and, thus, the model prediction is still acceptable and can be used to estimate the recovery rate of the ULPRO membrane system. As a result, it can be said that the experiments conducted employing the optimized input values validated the enhanced ULPRO model that had been formulated in this work.

4.4. Comparison with other previous model applied for ULPRO membrane

Comparison has been made between the result obtained using the enhanced DSPM-DE model with the solution diffusion model that has been applied on Vontron ULP32-8040 (Alawy & Salih 2016). The equations for the solution diffusion model were taken from Alawy & Salih (2016) and operating parameters in Table 1 with salt concentration at 2,000 ppm

Downloaded from http://iwaponline.com/wst/article-pdf/84/10-11/3372/967945/wst084103372.pdf
by guest

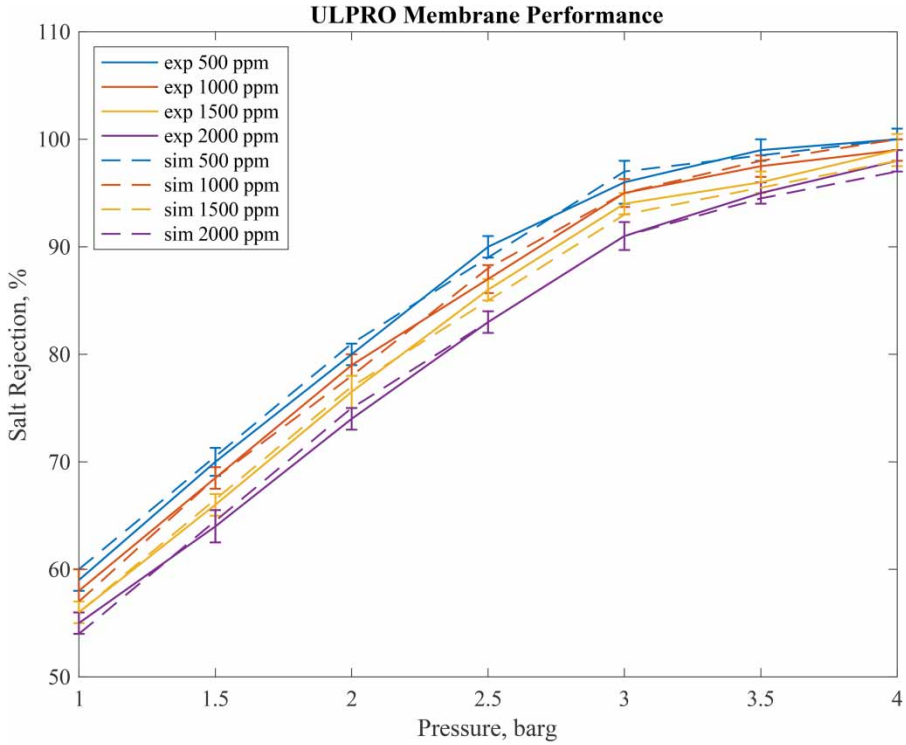

Figure 6 | Comparison of salt rejection between simulation and experiment on the ULPRO membrane.

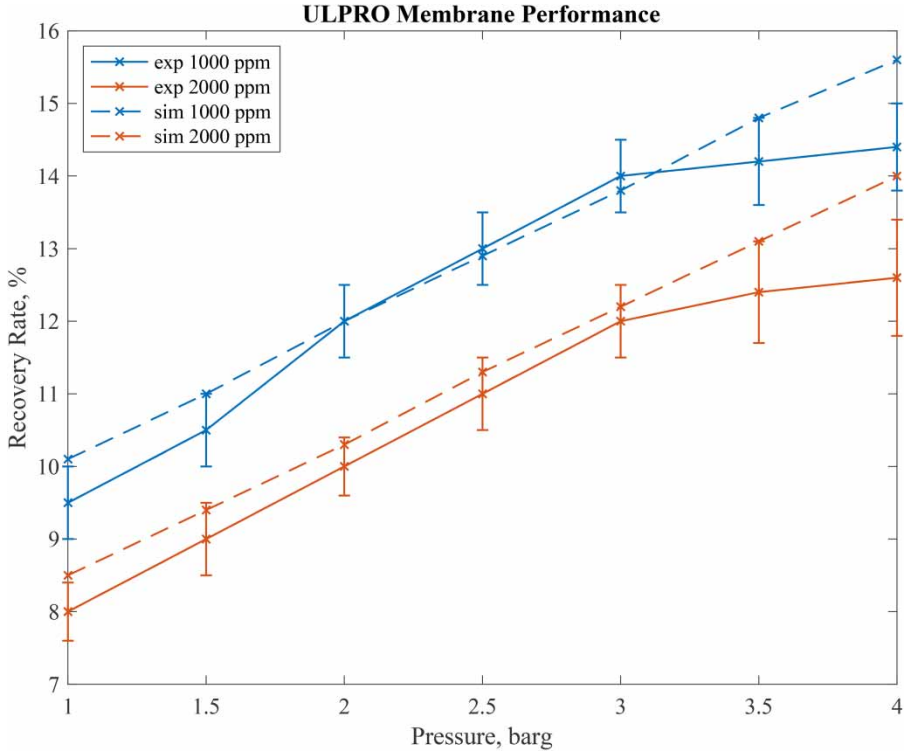

Figure 7 | Comparison of water recovery rate between simulation and experiment on the ULPRO membrane at NaCl concentrations of 1,000 ppm and 2000 ppm.

Downloaded from http://iwaponline.com/wst/article-pdf/84/10-11/3372/967945/wst084103372.pdf
by guest

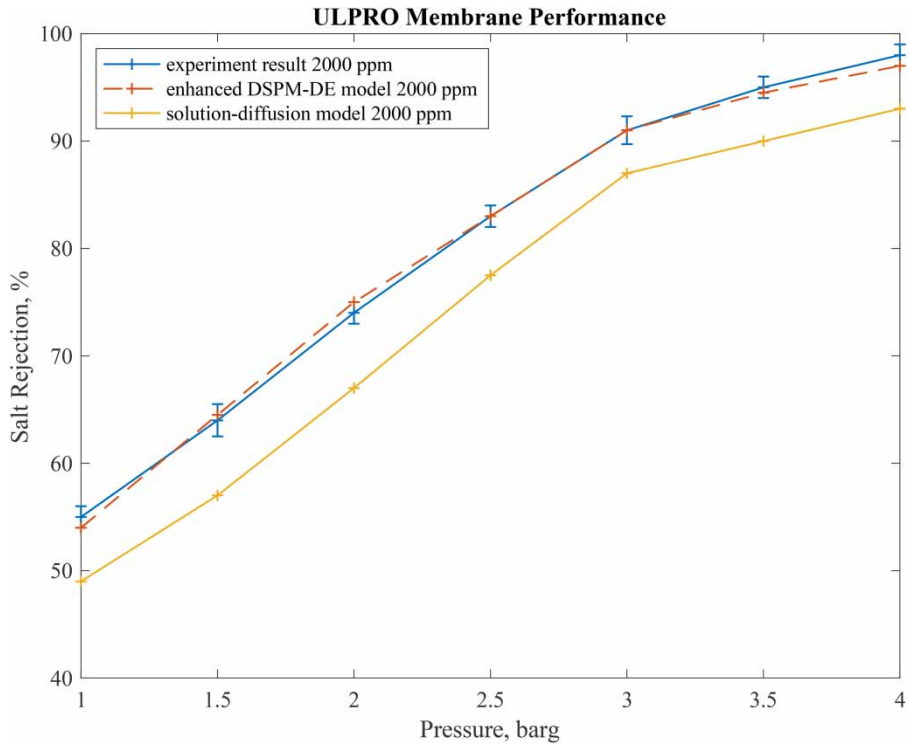

Figure 8 | Comparison of salt rejection between the enhanced DSPM-DE model, experiment and solution diffusion model on the ULPRO membrane at NaCl concentration of 2,000 ppm.

were applied. Figure 8 shows the salt rejection comparison between the enhanced DSPM-DE developed in this work, the experimental results and the solution diffusion transport model. The solution diffusion model shows a significant difference from the experimental results compared to the developed model. This is due to the fact that the solution diffusion model is not directly applicable to the membrane where pore processes such as physical sieving and Donnan exclusion are prevalent in dismissing solutes (Drewes *et al.* 2006). The Donnan equilibrium model accounts for both solute and membrane charge, resulting in a Donnan potential at the membrane surface due to co-ion repulsion and counter-ion attraction and causes the co-ions to repel. The counter-ions are also rejected since electroneutrality must be maintained (Judd & Jefferson 2003). However, in comparison with the enhanced formulated model, the solution diffusion model only considers a few parameters in the test to describe the transport mechanism. As a result, the assumption that the separation of solute and solvent is heavily reliant on the physical and chemical properties of the solution and the membrane reduces the quality of description of the transport mechanism. It can be said that the solution diffusion model disregards the membrane structure and the diffusive flow by assuming that the fluxes of the solute and solvent are controlled by the gradient of the driving forces.

This indicates that the solution diffusion model's applicability for NF membranes, specifically ULPRO type is relatively limited. This is also due to the porous nature of NF membranes, which means that pore flow is considerably more common and suitable for this ULPRO membrane. Nonetheless, Wijmans & Baker (1995) argued that the transport mechanism for NF membranes with pore radius between 0.5 to 1 nm could shift from pore-flow to sorption-diffusion. In other words, for certain solutes, the sorption-diffusion mechanism may be used to explain the transport process, whereas for others, the pore flow mechanism can be utilized. Therefore, it is crucial to validate the suitability of the membrane transport mechanism for that particular NF membrane, since there is a growing need to remove various types of pollutants from water and wastewater using membrane filtration.

5. CONCLUSIONS

An improved mathematical predictive model to theoretically predict the performance of the ULPRO membrane system at different feed pressure has been developed and validated through comparison between the results in simulation and experiments. Reliable prediction for the ULPRO model is essential in identifying the possible process options and operating

Downloaded from http://iwaponline.com/wst/article-pdf/84/10-11/3372/967945/wst084103372.pdf
by guest

limits to reduce development risk and time and thus can provide wider use of this cost-effective membrane technology in water treatment especially in the coastal region of Eastern Malaysia with ample availability of brackish water. In this study, the membrane characteristics and transport mechanism of the ULPRO membrane are explored using the enhanced DSPM-DE. Other than the steric effect, the Donnan effect also affects the performance of charged membranes. A negatively charged membrane attracts the opposite charged ions positive ions to its surface causes a high rejection rate. Moreover, analyses have also been done with the ULPRO membrane system by using MATLAB software tool to find the effect of applied pressure on the membrane performance. The mean squared error between the theoretical model and the experimental result for salt rejection and the water recovery rate is 0.6 and 0.5, respectively. In addition, based on the comparison made between the enhanced model with solution diffusion model, the result shows that our enhanced model predicts the membrane performance better. Since this enhanced model is developed considering all of the transport processes, it can be identified as an appropriate and accurate prediction model for the characterization of this particular ULPRO membrane separation system.

ACKNOWLEDGEMENTS

The financial support from the Selangor State Government Fund (Grant No. GA003-2020) is gratefully acknowledged.

DATA AVAILABILITY STATEMENT

All relevant data are included in the paper or its Supplementary Information.

REFERENCES

Abidi, A., Gherraf, N., Ladjel, S., Rabiller-Baudry, M. & Bouchami, T. 2016 Effect of operating parameters on the selectivity of nanofiltration phosphates transfer through a Nanomax-50 membrane. *Arabian Journal of Chemistry* **9**, S334–S341.

Agboola, O., Maree, J., Kolesnikov, A., Mbaya, R. & Sadiku, R. 2015 Theoretical performance of nanofiltration membranes for wastewater treatment. *Environmental Chemistry Letters* **13** (1), 37–47.

Ahn, K.-H., Song, K.-G., Cha, H.-Y. & Yeom, I.-T. 1999 Removal of ions in nickel electroplating rinse water using low-pressure nanofiltration. *Desalination* **122** (1), 77–84.

Al-Alawy, A. F. & Salih, M. H. 2016 Experimental study and mathematical modelling of zinc removal by reverse osmosis membranes. *Iraqi Journal of Chemical and Petroleum Engineering* **17** (3), 57–73.

Ali, N. A., Sidek, N. M. & Abdullah, I. 2014 Development of nanofiltration membrane separation prediction system for binary salt solutions. *Desalination and Water Treatment* **52** (4–6), 626–632.

Anderson, J. L. & Quinn, J. A. 1974 Restricted transport in small pores: a model for steric exclusion and hindered particle motion. *Biophysical Journal* **14** (2), 130–150.

Baker, R. W. 2012 *Membrane Technology and Applications*. New York, USA. John Wiley & Sons.

Bowen, W. & Mohammad, A. W. 1998 Characterization and prediction of nanofiltration membrane performance – a general assessment. *Chemical Engineering Research and Design* **76** (8), 885–893.

Bowen, W. R. & Welfoot, J. S. 2002a Modelling of membrane nanofiltration – pore size distribution effects. *Chemical Engineering Science* **57** (8), 1393–1407.

Bowen, W. R. & Welfoot, J. S. 2002b Modelling the performance of membrane nanofiltration – critical assessment and model development. *Chemical Engineering Science* **57** (7), 1121–1137.

Bowen, W. R. & Yousef, H. N. 2003 Effect of salts on water viscosity in narrow membrane pores. *Journal of Colloid and Interface Science* **264** (2), 452–457.

Carolyn, K., Junaidi, M., Hashim, N., Hussain, M., Mohamed Zuki, F., Mohamed Jan, B., Nasir, N. A. & Ahmad, A. L. 2020 Purification of lake water using a PES hollow fiber membrane. *Water Supply* **20** (2), 529–537.

Chai, X., Chen, G., Po-Lock, Y. & Mi, Y. 1997 Pilot scale membrane separation of electroplating waste water by reverse osmosis. *Journal of Membrane Science* **123** (2), 235–242.

Chew, C. M., Aroua, M. K., Hussain, M. A. & Ismail, W. M. Z. W. 2016 Evaluation of ultrafiltration and conventional water treatment systems for sustainable development: an industrial scale case study. *Journal of Cleaner Production* **112**, 3152–3163.

Dalwani, M., Benes, N. E., Bargeman, G., Stamatialis, D. & Wessling, M. 2011 Effect of pH on the performance of polyamide/polyacrylonitrile based thin film composite membranes. *Journal of Membrane Science* **372** (1–2), 228–238.

Davidson, M. G. & Deen, W. M. 1988 Hydrodynamic theory for the hindered transport of flexible macromolecules in porous membranes. *Journal of Membrane Science* **35** (2), 167–192.

Deen, W. 1987 Hindered transport of large molecules in liquid-filled pores. *AIChE Journal* **33** (9), 1409–1425.

Drewes, J., Bellona, C. & Xu, P. 2006 Viability of nanofiltration and reverse osmosis in removing emerging trace organic contaminants. *Paper presented at the 2006 AlChe Annual Meeting*, San Francisco, CA, USA.

Downloaded from http://iwaponline.com/wst/article-pdf/84/10-11/3372/967945/wst084103372.pdf
by guest

Ellison, W. 2007 Permittivity of pure water, at standard atmospheric pressure, over the frequency range 0–25 THz and the temperature range 0–100 °C. *Journal of Physical and Chemical Reference Data* **36** (1), 1–18.

Fei, W. & Bart, H.-J. 2001 Predicting diffusivities in liquids by the group contribution method. *Chemical Engineering and Processing: Process Intensification* **40** (6), 531–535.

Geraldes, V. & Alves, A. M. B. 2008 Computer program for simulation of mass transport in nanofiltration membranes. *Journal of Membrane Science* **321** (2), 172–182.

Gerard, R., Hachisuka, H. & Hirose, M. 1998 New membrane developments expanding the horizon for the application of reverse osmosis technology. *Desalination* **119** (1–3), 47–55.

Gray, S. R., Semiat, R., Duke, M., Rahardianto, A. & Cohen, Y. 2011 Seawater use and desalination technology. In: Wilderer, P. A. (ed.) *Treatise on Water Science*. Elsevier, pp. 73–109

Hafiz, M., Hawari, A. H., Alfahel, R., Hassan, M. K. & Altaee, A. 2021 Comparison of nanofiltration with reverse osmosis in reclaiming tertiary treated municipal wastewater for irrigation purposes. *Membranes* **11** (1), 32.

Hilal, N., Al-Zoubi, H., Darwish, N., Mohamma, A. & Arabi, M. A. 2004 A comprehensive review of nanofiltration membranes: treatment, pretreatment, modelling, and atomic force microscopy. *Desalination* **170** (3), 281–308.

Hussain, A. A., Abashar, M. E. E. & Al-Mutaz, I. S. 2006 Effect of ion sizes on separation characteristics of nanofiltration membrane systems. *Journal of King Saud University-Engineering Sciences* **19** (1), 1–18.

Imbrogno, A. & Schäfer, A. I. 2019 Comparative study of nanofiltration membrane characterization devices of different dimension and configuration (cross flow and dead end). *Journal of Membrane Science* **585**, 67–80.

Judd, S. & Jefferson, B. 2003 *Membranes for Industrial Wastewater Recovery and Re-use*. London, UK, Elsevier.

Kausley, S. B., Dastane, G. G., Kumar, J. K., Desai, K. S., Doltade, S. B. & Pandit, A. B. 2018 Clean water for developing countries: feasibility of different treatment solutions. In: Nriagu, J. *Encyclopedia of Environmental Health* (2nd Edition). Oxford, Elsevier, pp. 643–652.

Kondili, E. 2012 2.22 - Special Wind Power Applications. In: *Comprehensive Renewable Energy* (Sayigh, A. ed.). Elsevier, Oxford, pp. 725–746.

Koseoglu, H., Guler, E., Harman, B. I. & Gonulsuz, E. 2018 Water flux and reverse salt flux. In: Sarp, S. & Hilal, N. *Membrane-Based Salinity Gradient Processes for Water Treatment and Power Generation*. Elsevier, pp. 57–86.

Long, S. M. 2014 *Sarawak Coastal Biodiversity: A Current Status*.

Manson, A. A. A., Saleh, E., Mujahid, A. & Juneng, L. 2018 Temperature and salinity profiling analysis off Sarawak Waters, Malaysia. *Transactions on Science and Technology* **5** (3), 216–220.

Micari, M., Diamantidou, D., Heijman, B., Moser, M., Haidari, A., Spanjers, H. & Bertsch, V. 2020 Experimental and theoretical characterization of commercial nanofiltration membranes for the treatment of ion exchange spent regenerant. *Journal of Membrane Science* **606**, 118117.

Mohammad, A. W., Hilal, N., Al-Zoubib, H., Darwish, N. A. & Ali, N. 2007 Modelling the effects of nanofiltration membrane properties on system cost assessment for desalination applications. *Desalination* **206** (1–3), 215–225.

Mukherjee, N. 2014 *Nano Filtration (NF): Present Status and Challenges*. Retrieved from https://www.linkedin.com/pulse/20140704023849-105135096-nano-filtration-nf-present-status-and-challenges

Nguyen, L., Hai, F., Ibney., Kang, J., Price, W. E. & Nghiem, L. D. 2013 Removal of emerging trace organic contaminants by MBR-based hybrid treatment processes. *International Biodeterioration and Biodegradation* **85**, 474–482.

Oatley, D. L., Llenas, L., Pérez, R., Williams, P. M., Martínez-Lladó, X. & Rovira, M. 2012 Review of the dielectric properties of nanofiltration membranes and verification of the single oriented layer approximation. *Advances in Colloid and Interface Science* **173**, 1–11.

Obotey Ezugbe, E. & Rathilal, S. 2020 Membrane technologies in wastewater treatment: a review. *Membranes* **10** (5), 89.

Ozaki, H. 2004 Rejection of micropollutants by membrane filtration. Paper presented at the International Symposium on Membrane Technology 15–16 April 2004, Puteri Pan Pacific Hotel, Malaysia.

Ozaki, H., Sharma, K., Saktaywin, W., Wang, D. & Yu, Y. 2000 Application of ultra low pressure reverse osmosis (ULPRO) membrane to water and wastewater. *Water Science and Technology* **42** (12), 123–135.

Pan, S. Y., Haddad, A. Z., Kumar, A. & Wang, S. W. 2020 Brackish water desalination using reverse osmosis and capacitive deionization at the water-energy nexus. *Water Research* **183**, 116064.

Patrick, S. M. 2012 *The Coming Global Water Crisis*. Retrieved from https://www.theatlantic.com/international/archive/2012/05/the-coming-global-water-crisis/256896/

Pereira, D. A., Shah, A., Hasan, M. M., Ahmad, A., Alwi, A. T., Affan, S. & Lazim, Z. M. 2019 Saline water intrusion through Rajang river network due to sea level rise. *IOSR Journal of Mechanical and Civil Engineering* **16** (4), 55–65

Prayoga, A., Zakwan, M. & Bismo, S. 2021 Design of reverse osmosis filtration system for the supply of clean water from saltwater wells in tanjung lame village. *IOP Conference Series: Materials Science and Engineering* **1053** (1), 012124. IOP Publishing.

Roy, Y. & Sharqawy, M. H. 2015 Modeling of flat-sheet and spiral-wound nanofiltration configurations and its application in seawater nanofiltration. *Journal of Membrane Science* **493**, 360–372.

Shenvi, S. S., Isloor, A. M. & Ismail, A. F. 2015 A review on RO membrane technology: developments and challenges. *Desalination* **368**, 10–26.

Sidek, N., Ali, N., Abdullah, I. & Draman, S. 2014 Development of nanofiltration membrane separation prediction system: interacting effect of steric and Donnan factors. *Desalination and Water Treatment* **52**, 626–632.

Downloaded from http://iwaponline.com/wst/article-pdf/84/10-11/3372/967945/wst084103372.pdf
by guest

Van der Bruggen, B. & Vandecasteele, C. 2003 Removal of pollutants from surface water and groundwater by nanofiltration: overview of possible applications in the drinking water industry. *Environmental Pollution* **122** (3), 435–445.

Van der Bruggen, B., Koninckx, A. & Vandecasteele, C. 2004 Separation of monovalent and divalent ions from aqueous solution by electrodialysis and nanofiltration. *Water Research* **38** (5), 1347–1353.

Vontron Technology Co., Ltd. 2016 *Manual of Product, Technical Support and Service*. Vontron Technology Co., Ltd.

WHO (World Health Organization) 2011 *Guidelines for Drinking-Water Quality* (4th edn). World Health Organization, Geneva, Switzerland.

Wijmans, J. G. & Baker, R. W. 1995 The solution-diffusion model: a review. *Journal of Membrane Science* **107** (1–2), 1–21.

Wong, J. 2020 Sarawak to spend RM18b on water supply projects. *The Star*. Retrieved from: https://www.thestar.com.my/business/business-news/2020/12/14/sarawak-to-spend-rm18b-on-water-supply-projects

Xie, D. 2011 An improved approximate Newton method for implicit Runge–Kutta formulas. *Journal of Computational and Applied Mathematics* **235** (17), 5249–5258.

Xu, P., Drewes, J. E. & Heil, D. 2008 Beneficial use of co-produced water through membrane treatment: technical-economic assessment. *Desalination* **225** (1–3), 139–155.

Yusof, K., Azid, A., Sani, M. S. A., Samsudin, M. S., Amin, S., Rani, N. & Jamalani, M. A. 2019 The evaluation on artificial neural networks (ANN) and multiple linear regressions (MLR) models over particulate matter (PM10) variability during haze and non-haze episodes: a decade case study. *Malaysian Journal of Fundamental and Applied Sciences* **15**, 164–172.

First received 30 June 2021; accepted in revised form 21 September 2021. Available online 5 October 2021

Downloaded from http://iwaponline.com/wst/article-pdf/84/10-11/3372/967945/wst084103372.pdf
by guest